Flat bands in twisted bilayers of polar two-dimensional semiconductors

Xing-Ju Zhao,[1] Yang Yang,[2] Dong-Bo Zhang,[1,3,*] and Su-Huai Wei[2,†]
[1]Department of Physics, Beijing Normal University, Beijing 100875, China
[2]Beijing Computational Science Research Center, Beijing 100193, China
[3]College of Nuclear Science and Technology, Beijing Normal University, Beijing 100875, China

(Received 20 June 2020; revised 2 November 2020; accepted 15 January 2021; published 29 January 2021)

We investigate the Bloch flat bands in twisted bilayers from nonpolar to polar two-dimensional semiconductors using first-principles calculations and density functional based tight-binding simulations. First, to delineate the underlying mechanism of the formation of the flat bands, we rely on a tight-binding model of modified graphene where a bias between the A-B sublattice of the hexagonal lattice is introduced. By analyzing the evolution of the valence and conduction band edges of the bilayer of the modified graphene with different stacking patterns, a mechanism attributed to the splitting of the defect-like band edge states induced by different stacking patterns is revealed. The magic angle mechanism is no longer needed. Next, guided by the revealed mechanism, we predict the formation of flat bands in twisted bilayers of a series of two-dimensional systems from nonpolar to polar semiconductors. Our finding has important implications for exploring the flat band physics in low dimensions.

DOI: 10.1103/PhysRevMaterials.5.014007

I. INTRODUCTION

In condensed matters, an unusual characteristic of Bloch electrons is the existence of flat bands. Being weakly dispersive, a flat band has a vanishingly small band width (W) and accordingly, high density of states, inducing strong Coulomb interactions (U) between electrons, i.e., $U \gg W$. If the flat band is at the Fermi level, because the kinetic energy of the electrons confined by W is much smaller than the Coulomb interaction, the associated system may exhibit pronounced correlation effects [1,2], as already seen in various exotic quantum states. These include superconductivity [3], ferromagnetism [4], Wigner crystal [5], and zero-magnetic field fractional quantum Hall effects (QHE) of Bloch states [6–10]. Since flat bands provide a route to accessing correlated electronic states, searching for new materials with flat bands is important and currently under active investigations.

As one of the most important degree of freedom, twist have been used as an effective strategy to modulate the physical or chemical properties in low-dimensional materials [11–15]. Recent theoretical and experimental advances have shown that such flat bands could be obtained in twisted van der Waals (vdW) heterostructures assembled from atomically thin two-dimensional (2D) crystals [13–15]. Due to the twist-induced misalignment between constituent layers, a twisted vdW heterostructures will develop complex lateral morphologies usually showing as a moiré pattern with periodicity much longer than the interatomic distance. This special moiré superlattice creates strong modulation on the electronic interlayer coupling, leading to interesting physics such as the observation of Hofstadter butterfly [16,17], fractional QHE [18], gap opening [19], and moiré excitons [20–23]. Particularly, the electronic structure of twisted bilayer graphene (TBG) can be tailored to develop isolated flat bands at some magic angles [24–27]. Furthermore, it has also been shown that the value of magic angles relies on the interlayer coupling that can be tuned by varying the interlayer spacing with hydrostatic pressure [28,29] or by applying bias potential [30]. Experiments have shown that these flat bands are the key to achieve the correlated insulating and superconductive phases in graphene systems [13–15].

Different from graphene, 2D polar crystals with a broken A-B sublattice symmetry usually have a band gap. Consequently, when they form the twisted bilayer, the low energy electronic states are of different behaviors with respect to TBG. Therefore it is interesting to explore the formation of flat bands in this category of materials. Although several studies on the twisted bilayers of polar systems [31–33] have explored the possibility of the existence of flat bands, a systematic study is needed to clarify the impact of the polarity variation on the formation of flat bands. This is the main purpose of the present work.

This paper is summarized as follows. First, we illustrate the mechanism leading to the formation of flat bands in a twisted bilayer of 2D polar semiconductors. This is achieved by performing the density functional based tight-binding (DFTB) calculations of twisted bilayer of modified graphene where a bias between the A-B sublattice of the hexagonal lattice is introduced. By varying the strength of the bias, we witness the emergence of the isolated flat bands. This represents a new mechanism due to the polarity and is different from the magic angle mechanism of the twisted bilayer graphene. Along this line, by analyzing the evolution of the valence and conduction band edge states of the bilayer with different stacking patterns of the twisted bilayer of biased graphene, we further show that the formation of flat bands can be understood as the consequence of the splitting of the defect-like band edge states induced by different stacking patterns. Second, guided by this

*dbzhang@bnu.edu.cn
†suhuaiwei@csrc.ac.cn

new mechanism, we successfully predict the existence of flat bands in twisted bilayers of a series of 2D materials with polarities vary from weak to strong.

II. METHODS

In the modified graphene model (see more details in the Appendix), a bias between the A-B sublattice of the hexagonal lattice is applied by scaling the on-site p orbital energy E_p of atoms situated on the A sublattice. Here, a direct first-principle calculation of the band structure of the modified TBG to observe the formation of flat bands is difficult because of the huge number of atoms in the unit cell of the moiré superlattice. For example, at the first magic angle, $\theta \approx 1.08^\circ$, there are 11 164 atoms inside the unit cell. However, it is known that the magic angle varies with the interlayer distance of the TBG [28,29], such as at an interlayer distance of 2.80 Å, the corresponding magic angle increases to $\theta \approx 2.28^\circ$ and the size of the unit cell is substantially reduced to 2524 atoms, which is treatable using the DFTB method (where local orbital basis [34,35] was employed for the band structure calculations). Therefore, in the modified graphene model, we will adopt $d = 2.80$ Å to carry out the qualitative study of the evolvement of the flat band formation as a function of the twisted angle and asymmetry of the A-B sublattice.

Except for the modified graphene model, all the other 2D systems were treated by first-principles approaches [36] as implemented in the VASP [37] code. The interactions of the valence electrons with the ionic cores were described by the projector augmented wave (PAW) [38] method. For the exchange-correlation functional, we use the generalized gradient approximation of Perdew, Burke, and Ernzerhof [39]. The Brillouin zone of various simple stacking bilayers were sampled with a dense k-point mesh of $31 \times 31 \times 1$ and an energy cutoff of 500 eV were used for the cut-off of the basis functions. While for twisted moiré superlattice, the Brillouin zone is sampled at the Γ point to obtain the self-consistent charge density. All the electronic iteration was converged to 10^{-5} eV. The lattice constant and the atomic position of the monolayer unit cell were fully relaxed by the conjugate gradient method until all the residual force components were less than 0.01 eV/Å. All these parameters have been carefully examined to ensure good convergence. The twisted moiré superlattice were constructed based on the fully relaxed unit cell and kept rigid during the band structure calculation. For the interlayer distance, the vdW interaction is depicted by adding extra dispersive forces. Unless otherwise specified, the layer distance was fixed to be at the averaged value of the minimum and maximum of the layer distance of various simple stacking patterns included in their corresponding moiré superlattice, for instance, $d = \frac{1}{2}(d_{AB} + d_{AA})$, where d_{AB} is the layer distance of AB stacking and d_{AA} is the layer distance of AA stacking appeared in the moiré superlattice.

III. RESULTS AND DISCUSSION

A. The formation of flat bands in a modified graphene model

Here, we illustrate the mechanism leading to the formation of flat bands in a twisted bilayer of 2D polar semiconductors by carrying out DFTB calculations of a modified graphene model. In this model, a gradually increased bias between the A-B sublattice of the hexagonal lattice is introduced to mimic a polar system with a polarity change from weak to strong. Such a bias breaks the A-B sublattice symmetry and thus opens a band gap in the whole Brillouin zone of the monolayer graphene.

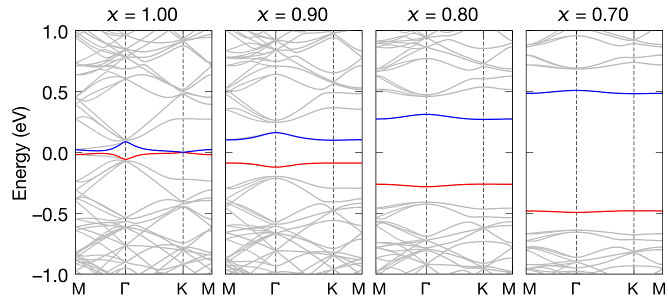

FIG. 1. Energy bands of the modified TBG at twist angle $\theta = 2.88^\circ$ with different scaling factor x for the on-site p orbital energy (E_p) of the elements for A sublattice.

Specifically, the bias between the A-B sublattice is imposed by scaling the on-site p orbital energy E_p of atoms situated on the A sublattice with a factor x, where $0.70 \leqslant x \leqslant 1.00$. Consider a non-magic twist angle $\theta = 2.88^\circ$, we examine the evolution of the band structure of TBG with x. In this paper, we define the flat band as the band have a bandwidth less that 15 meV. Because $\theta = 2.88^\circ$ is not a magic angle, the band structure at $x = 1.00$ (no bias) does not have flat bands, Fig. 1. The band structures of the TBG with $x = 0.90$, $x = 0.80$, and $x = 0.70$ are also shown, revealing that as x decreases (i.e., the difference in on-site energy between A and B sublattices increases), the band gap increases and the bands around the Fermi level are now isolated and display a gradual flattening behavior. At $x = 0.70$, these bands are nearly flat with a small bandwidth of 12 meV. This result reveal that the formation of flat bands is due to the presence of a bias, or equivalently, the presence of polarity.

To understand the mechanism of formation of flat bands in TBG, we analyze the stacking effect of the moiré superlattice. For the TBG with $x = 0.70$, there are one AA stacking area and two Bernal $B^{CC'}$ stacking areas, see Figs. 2(a) and 2(b). We have calculated the band structures of pure AA and $B^{CC'}$ graphene bilayers. For the convenience of comparison with the TBG, these calculations were performed with a cell size comparable with the moiré superlattice.

Compared to $B^{CC'}$ stacking, the valence (conduction) band edge of AA stacking is higher (lower) in energy, Fig. 2(c). As a result, the valence band maximum (VBM) and conduction band minimum (CBM) states of the TBG should energetically prefer to reside within the AA stacking region of the moiré superlattice. This can be demonstrated by visualizing the spatial charge distribution of the band edge states. As shown in Figs. 2(d) and 2(e), the charge distributions of both VBM and CBM states at the high-symmetry $k = K$ are both localized within the AA stacking area. Such localized behavior of electrons further reveals that the obtained flat band states are defectlike localized states.

The above analysis hints that the formation of flat bands is essentially due to the interlayer stacking-induced state

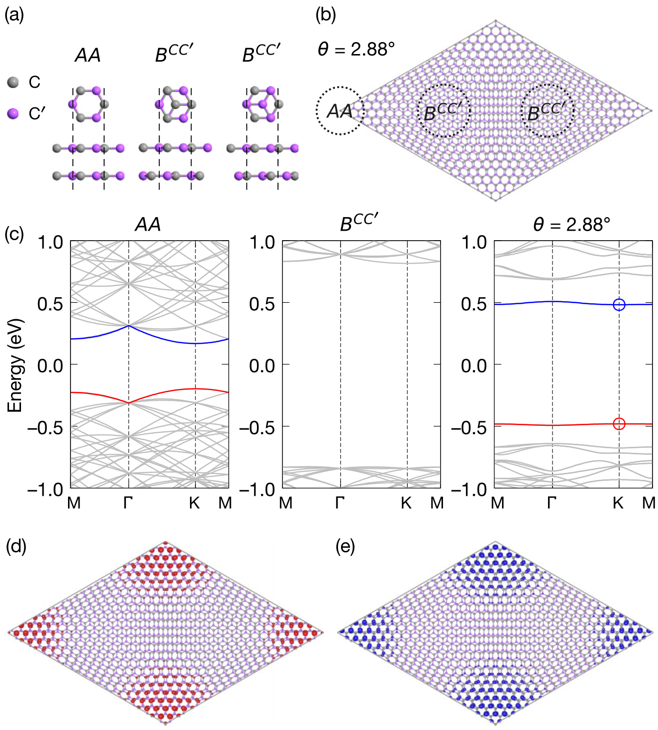

FIG. 2. (a) Modified graphene bilayers with *AA* stacking and two Bernal stackings. (b) Modified TBG with breaking sublattice symmetry ($x = 0.70$) at the twist angle $\theta = 2.88^\circ$. (c) Energy bands of graphene bilayers with *AA* stacking, Bernal stacking $B^{CC'}$, and modified TBG with $\theta = 2.88^\circ$. [(d) and (e)] Electronic density distribution of the valence band edge and conduction band edge state at $k = K$ as marked by circles in (c)[right].

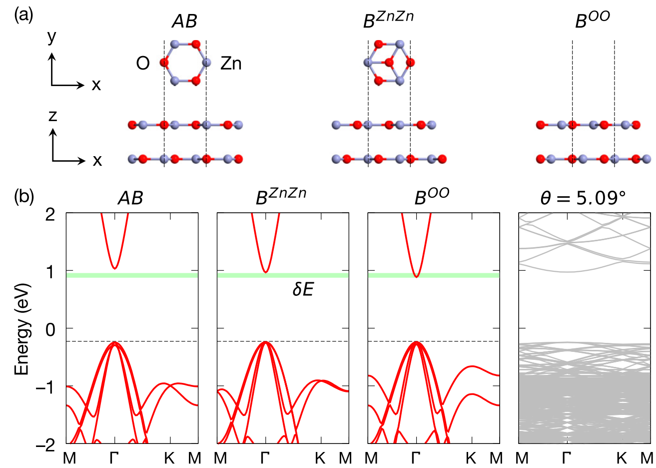

FIG. 3. (a) ZnO bilayers with *AB* stacking and two Bernal stackings, B^{ZnZn} and B^{OO}. The red and light blue atoms corresponding to O and Zn atoms, respectively. (b) Energy bands of ZnO bilayers with *AB* stacking, B^{ZnZn} Bernal stacking, B^{OO} Bernal stacking, and twisted ZnO bilayer with a twist angle $\theta = 5.09^\circ$. The color shaded rectangle mark the energy order difference δE between different stacking patterns.

localization. This fact reminds us that we can predict the existence of flat bands in a twisted bilayer system by only examining the energy order of the VBM and CBM states in the bilayers with different stacking patterns. With the polarity of the system change, the energy order of the VBM and CBM states between different stacking patterns may have a significant difference, which could largely influence the appearance of the flat band. With this as a guidance, we study the formation of flat bands in the twisted bilayers of various 2D systems, with a polarity vary from weak to strong.

B. Energy bands in weak polar twisted bilayer ZnO

2D binary compound ZnO has a planar structure, with a band gap, and has been confirmed as a novel weak polar structure [40]. Thus it can be exactly used to check the validity of our theory evolve with the system polarity. In Fig. 3(a), three representative stacking patterns (*AB*, B^{ZnZn}, and B^{OO}) appear in the twisted moiré superlattice are presented with both the top and side view. And their corresponding energy band structures calculated by the first-principle simulation are also shown in Fig. 3(b). We can see that the energy order difference δE [color shaded in Fig. 3(b)] between different stacking patterns (*AB*, B^{ZnZn}, and B^{OO}) is very small, such as 79 meV for CBM state. This is a sign that the interlayer stacking effect has little impact on the electronic structure for ZnO layers.

These features hint that the states corresponding to different stacking patterns may not be separate. As a result, there may be no isolated flat band formed. To check this, we use the twisted bilayer of ZnO with $\theta = 5.09^\circ$ as an example. The band structure displayed in Fig. 3(b) shows that there is no isolated flat band formed neither in VBM nor CBM states, indeed.

Due to the small energy order difference between different stacking patterns, there is no flat band formed in the moiré superlattice with a twist angle $\theta = 5.09^\circ$. The natural question is, if we continually reduce the twist angle, what will the edge state evolve? To elucidate this issue, we calculated the band width of a series of twist angles, such as $\theta = 5.09^\circ$, 4.41°, 3.89°, 3.48°, and 3.14°, et al. Our simulations confirm that the VBM states always tangle with other near energy bands. While the CBM state gradually isolated from other bands. Such as for $\theta = 5.09^\circ$ and 4.41°, the CBM state still tangle with its nearest high level energy bands, while for $\theta = 3.89^\circ$, the CBM state isolated from the other conduction energy bands (E_{isolate}) of 7 meV, and for $\theta = 3.14^\circ$, E_{isolate} increase to 15 meV. Additionally, the band width of the CBM state change from 182, 136, 104, 81 to 64 eV for $\theta = 5.09$, 4.41°, 3.89°, 3.48°, and 3.14°, respectively, see Table I. Even smaller θ would generate very flat isolated VBM bands, however this exceed the efficient simulation of DFT, due to the rapidly increase number of atoms in the supercell, Table I. From the above modified graphene and ZnO examples, we can predict that the formation of flat bands closely related to the energy order difference δE of the edge states between different stacking patterns, or the system polarity.

C. Flat bands in twisted bilayer of transition metal dichalcogenides

Transition metal dichalcogenides MX_2 (M = Mo, Cr, W; X = S, Se) represent an important class of 2D materials. Using

TABLE I. Information of the moiré superlattice and its corresponding band structure properties. θ, N, (m, n), $E_{\rm isolate}$, and W are the twisted angle, the total number of atoms in the superlattice, the moiré superlattice index [41,42], the CBM state isolated from the other conduction energy bands, and the CBM band width, respectively.

θ (°)	N	(m, n)	$E_{\rm isolate}$ (meV)	W (meV)
5.09	508	(6,7)	–	182
4.41	676	(7,8)	–	136
3.89	868	(8,9)	7	104
3.48	1084	(9,10)	12	81
3.14	1324	(10,11)	15	64

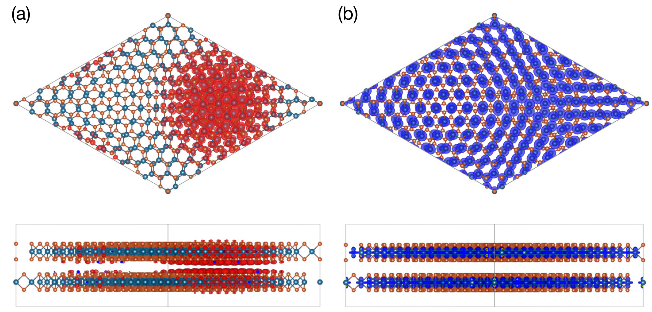

FIG. 5. Electron density distribution of (a) the valence band edge state and (b) the conduction band edge state at $k = K$. The top and bottom panels correspond to the top and side views, respectively.

twisted bilayer MoS_2 as an example, we analyze the existence of flat bands. Being a polar system, the ground state of the MoS_2 bilayer adopts a AB stacking where the Mo atoms in one layer are on top of the S atoms in another layer, and vice versa, Fig. 4(a). The twisted moiré superlattice obtained by twisting this AB stacking consists of three different regions characterized by different stacking patterns, labeled as AB, $B^{\rm MoMo}$, and $B^{\rm SS}$, Figs. 4(a)–4(c). However, different from single atomic layer such as ZnO, the monolayer MoS_2 unit cell has two S atoms reside out of the Mo plane with inversion symmetry. This has consequence on the interlayer interaction.

For the $B^{\rm MoMo}$ stacking, we find one Mo atom in one layer that is on top of the other Mo atom in the other layer. The distance between these two Mo atoms is $d_{\text{Mo-Mo}} = 6.15$ Å [Fig. 4(b)]. For the $B^{\rm SS}$ stacking, we identify one S atom in one layer on top of the other S atom in the other layer. The distance between these two S atoms is $d_{\text{S-S}} = 3.02$ Å [Fig. 4(c)]. For the AB stacking, we identify one Mo atom in one layer on top of one S atom in the other layer. The distance between these two atoms is $d_{\text{Mo-S}} = 4.58$ Å [Fig. 4(a)]. Therefore, due to the relatively large interatomic separations of $d_{\text{Mo-Mo}}$ and $d_{\text{Mo-S}}$, the interaction between these atoms is rather weak. On the contrary, $d_{\text{S-S}}$ is relatively small such that the interlayer interaction between S atoms in both layers is more significant.

Figure 4(d) shows the band structures of the bilayer MoS_2 with AB, $B^{\rm MoMo}$, and $B^{\rm SS}$ stacking patterns, respectively. We can see that the valence band edge at Γ point of $B^{\rm SS}$ stacking is higher than those of AA or $B^{\rm MoMo}$ stacking patterns. Therefore, flat bands in the twisted bilayer MoS_2 should originate from these states located around the $B^{\rm SS}$ stacking region. As a demonstration, we have calculated the band structure of the twisted bilayer MoS_2 with a twist angle $\theta = 5.09°$, as shown in Fig. 4(d). Indeed, we see the VBM bands are isolated and flat with a band width $W = 11$ meV. Moreover, Fig. 5(a) shows that the charge distribution of the VBM state at high-symmetry $k = K$ point is localized within the $B^{\rm SS}$ stacking region. Fig. 5(a) [lower panel] shows that these states are from S atoms, also confirming that these flat band states are due to the stacking effect from $B^{\rm SS}$ stacking regions. It is also useful to point out that compared to the localized VBM states, the CBM states of the twisted bilayer MoS_2 are extensive. They essentially stay on Mo atoms, Fig. 5(b). As aforementioned, the distance between Mo atoms in both monolayers are rather large. The weak interlayer interaction via Mo atoms has a little impact on the electronic states.

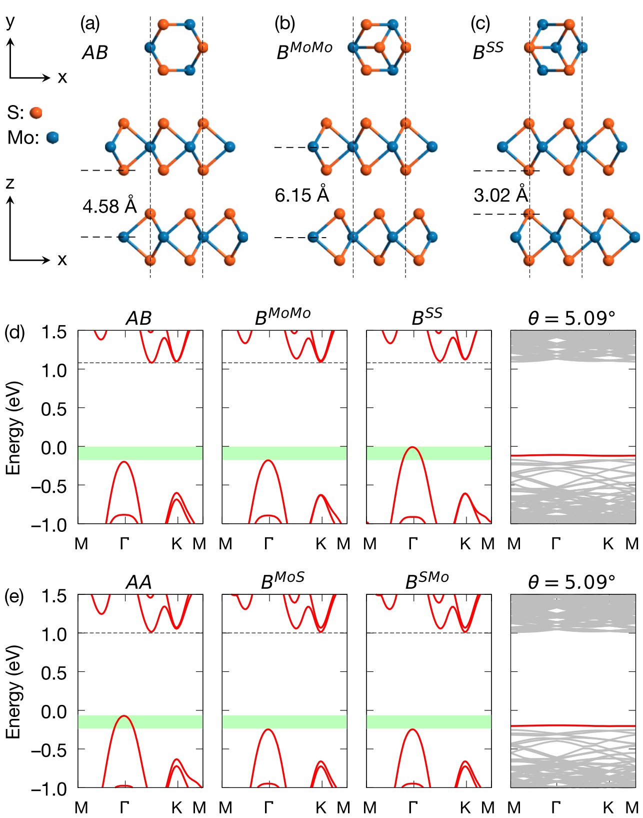

FIG. 4. [(a)–(c)] MoS_2 bilayers with AB stacking and two Bernal stackings, $B^{\rm MoMo}$ and $B^{\rm SS}$. (d) Energy bands of MoS_2 bilayers with AB stacking, $B^{\rm MoMo}$ Bernal stacking, $B^{\rm SS}$ Bernal stacking, and twisted MoS_2 bilayer with a twist angle $\theta = 5.09°$. (e) Energy bands of MoS_2 bilayers with AA stacking, $B^{\rm MoS}$ Bernal stacking, $B^{\rm SMo}$ Bernal stacking, and twisted MoS_2 bilayer with a twist angle $\theta = 5.09°$.

The twisted bilayer MoS_2 can be also obtained by twisting the MoS_2 bilayer with AA stacking where S atoms in one layer are on top of the S atoms in the other layer. Similarly, by comparing the band alignments of the VBM states at Γ point for the MoS_2 bilayers with AA stacking, $B^{\rm MoS}$ stacking, and $B^{\rm SMo}$ stacking, Fig. 4(e), we conclude that flat bands may emerge near the VBM of the twisted bilayer MoS_2. This is confirmed by our band structure calculations of a twisted

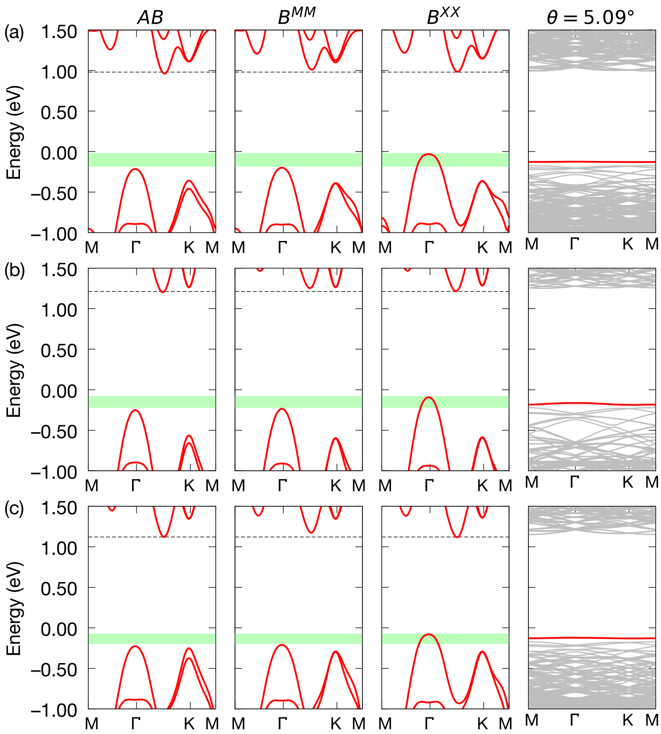

FIG. 6. Energy bands of (a) $MoSe_2$, (b) WS_2, and (c) WSe_2 bilayers with AB stacking, two Bernal stackings, and twisted moiré superlattice with a twist angle $\theta = 5.09°$.

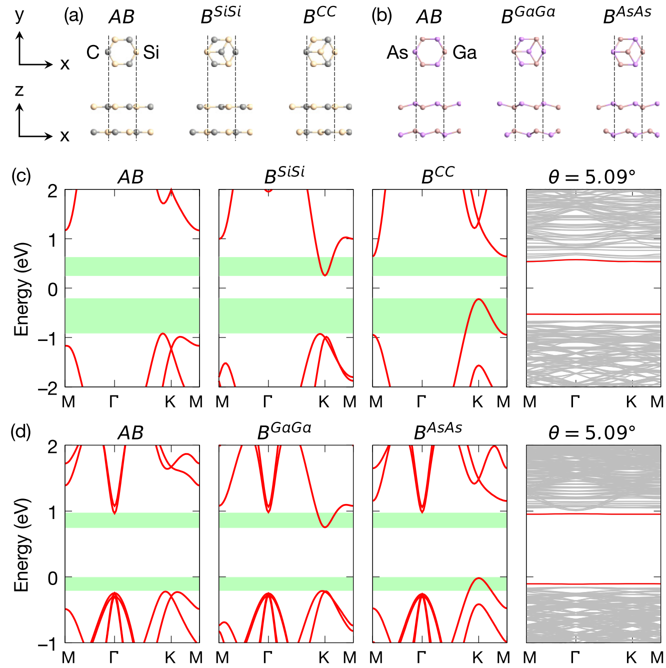

FIG. 7. (a) Planar SiC bilayers with AB stacking and two Bernal stackings. (b) Low-buckled GaAs bilayers with AB stacking and two Bernal stackings. (c) Energy bands of SiC with AB stacking, two Bernal stackings, and twisted moiré superlattice with a twist angle $\theta = 5.09°$. (d) Energy bands of GaAs with AB stacking, two Bernal stackings, and twisted moiré superlattice with a twist angle $\theta = 5.09°$.

bilayer MoS_2 with a twist angle $\theta = 5.09°$, Fig. 4(e) [right]. Similar results can be also obtained in the twisted bilayers of other transition metal dichalcogenides MX_2 (M = Mo, Cr, W; X = S, Se), Fig. 6.

Here we notice that at very small twist angles (such as $\theta < 1°$) TMD homo- and heterobilayers will relax into large domains with commensurate stacking patterns separated by narrow domain walls [43–45]. The width of the domain walls are about 3 nm, which are still large enough to separate different stacking patterns. Thus the defectlike flat band mechanism maybe still valid in this situation, while this need to be further confirmed.

D. Flat bands in twisted bilayers of other 2D materials

The binary group IV-IV and group III-V compounds may also form layered materials. For example, Sahin *et al.* [46] predicted that the binary IV-IV compounds and the group III-V compounds can form various layered honeycomb structures. These materials are of potential applications in various areas. Here, we take SiC and GaAs as examples to elucidate the formation of flat bands in the twisted bilayers of these systems. For SiC, the possible stacking patterns of the bilayer form is shown in Fig. 7(a). The corresponding band structures are shown in Fig. 7(c). We find that the VBM (CBM) states at $k = K$ of the B^{CC} (B^{SiSi}) bilayer is higher (lower) than those of AB and B^{SiSi} (B^{CC}) bilayers. Accordingly, the VBM (CBM) states of the twisted bilayer form flat bands, Fig. 7(c)[right]. On the other hand, for GaAs, the possible stacking patterns of the bilayer form is shown in Fig. 7(b). The corresponding band structures are shown in Fig. 7(d). We find that the CBM states at $k = K$ of the B^{GaGa} bilayer is lower than those of AB and B^{AsAs} bilayers, and the VBM states at $k = K$ of the B^{AsAs} bilayer is higher than those of AB and B^{GaGa} bilayers. Therefore both CBM and VBM states of the twisted bilayer form flat bands, Fig. 7(d) [right]. In general, we see that in these polar system, the flat band near the CBM is formed with charge localized in the $B^{\text{cation-cation}}$ region because the cation-cation bonding state has the lowest energy than other unoccupied states, whereas the flat band near the VBM is formed with charge localized in the $B^{\text{anion-anion}}$ region, because the anion-anion antibonding state has the highest energy than other occupied states.

IV. CONCLUSION

In summary, using a modified graphene model and DFTB calculations, we illustrate that the emergence of flat bands in twisted bilayer of 2D polar semiconductors is due to the polarity. The polarity mechanism, combining the effect of stacking patterns, induces the splitting of the defect-like band edge states, giving rise to the formation of isolated bands in the twisted bilayer. As long as the distance between the localized region is larger than the localization radius, i.e., the twist angle is sufficiently small, these isolated bands will become very flat and no magic angles are needed. With this new mechanism, using first-principles calculations, we successfully predict the existence of flat bands in twisted bilayers of a series of polar 2D materials, with polarities vary from weak to strong. For weak polar system, a small twist angle is needed to form flat bands; while for strong polar system, even larger twist angle is needed. This is because the weak polar corresponding to shallow potential well always need a larger size of spacial distance to separate the different states. Our results, open a new route to explore the flat bands and the associated many-body physics in 2D materials.

ACKNOWLEDGMENTS

This work was supported by the MOST of China (Grant No. 2017YFA0303400) and NSFC under Grants No. 11674022, No. 11991060, No. 51672023, No. 11634003, and No. U1930402. D.-B.Z. was supported by the Fundamental Research Funds for the Central Universities. X.-J.Z. was supported by the Postdoctoral Innovative Talent Support Program (BX201700025).

APPENDIX: MODIFIED GRAPHENE MODEL

Under the framework of a tight-binding approximation, the π electron energy levels or bands calculation is simple and can largely represent the transport or other solid state properties. In this model, the Bloch function of each atom in the unit cell can be wrote as the linear combination of atomic wave function. By solving the secular equation $\det[H - ES] = 0$, we can easily obtain the eigenvalue of any given $\boldsymbol{k}$ point in the first Brillouin zone [47].

For native graphene with real space unit cell vectors $\boldsymbol{a}_1 = (\frac{\sqrt{3}}{2}a, \frac{a}{2})$, $\boldsymbol{a}_2 = (\frac{\sqrt{3}}{2}a, -\frac{a}{2})$ and reciprocal lattice vectors $\boldsymbol{b}_1 = (\frac{2\pi}{\sqrt{3}a}, \frac{2\pi}{a})$ and $\boldsymbol{b}_2 = (\frac{2\pi}{\sqrt{3}a}, -\frac{2\pi}{a})$, we have [47]

$$H = \begin{bmatrix} \epsilon_{2p} & tf(\boldsymbol{k}) \\ tf(\boldsymbol{k})^* & \epsilon_{2p} \end{bmatrix}, \quad S = \begin{bmatrix} 1 & sf(\boldsymbol{k}) \\ sf(\boldsymbol{k})^* & 1 \end{bmatrix}. \tag{A1}$$

where H and S are the transfer and overlap matrix, ϵ_{2p} is the orbital energy of the $2p$ level, which is also the on-site energy of the C atom. t and s are the transfer and overlap integral which can be empirically parameterized. $f(\boldsymbol{k})$ is a function of $\boldsymbol{k}$ points which is also correlated with the atomic coordinates in the unit cell. By solving the secular equation $\det[H - ES] = 0$, we get

$$(\epsilon_{2p} - E)^2 - |f(\boldsymbol{k})|^2 (t - Es)^2 = 0 \tag{A2}$$

and then,

$$\epsilon_{2p} - E = \pm\omega(\boldsymbol{k})(t - Es). \tag{A3}$$

In the nearest-neighbor approximation, where

$$\omega(\boldsymbol{k}) = \sqrt{|f(\boldsymbol{k})|^2} = \sqrt{1 + 4\cos\frac{\sqrt{3}k_x a}{2}\cos\frac{k_y a}{2} + 4\cos^2\frac{k_y a}{2}} \tag{A4}$$

so,

$$E = \frac{\epsilon_{2p} \pm t\omega(\boldsymbol{k})}{1 \pm s\omega(\boldsymbol{k})}. \tag{A5}$$

At K point,

$$\boldsymbol{k} = \left(\frac{2}{3}\boldsymbol{b}_1 + \frac{1}{3}\boldsymbol{b}_2\right) = \left(\frac{2\pi}{\sqrt{3}a}, \frac{2\pi}{3a}\right)$$

thus we obtain $w(\mathrm{K}) = 0$, and $E(\mathrm{K}) = \epsilon_{2\mathrm{p}}$ for both π bonding band and π^* antibonding band, which is symmetrical around the K point, and no energy gap is presented.

In the modified graphene model, we artificially modify on-site $2p$ orbital energy to ϵ'_{2p} of one atom in the unit cell and keep all the other parameters untouched, then in the modified graphene model the Hamilton matrix can be written as

$$H = \begin{bmatrix} \epsilon_{2p} & tf(\boldsymbol{k}) \\ tf(\boldsymbol{k})^* & \epsilon'_{2p} \end{bmatrix} \tag{A6}$$

thus,

$$(\epsilon_{2p} - E)(\epsilon'_{2p} - E) - |\omega(\boldsymbol{k})|^2 (t - Es)^2 = 0. \tag{A7}$$

There is no analytical solution. Luckily, here we only need to consider the K point situation. Substitute $w(\mathrm{K}) = 0$ into Eq. (A7), we get two bands at K with $E = \epsilon_{2p}$ and ϵ'_{2p}, thus a gap $E_{\text{gap}} = |\epsilon_{2p} - \epsilon'_{2p}|$ is opened in the modified graphene model around the K point.

In our simulation code DFTB+ [34,35], the modified graphene model with a bias between the A-B sublattice of the hexagonal lattice can be realized by scaling the on-site $2p$ orbital energy $\epsilon_{2\mathrm{p}}$ of atoms situated on the A sublattice, which can be easily achieved by modifying the on-site energy parameter in the Slater-Koster files.

[1] W. Kohn and J. M. Luttinger, New Mechanism for Superconductivity, Phys. Rev. Lett. **15**, 524 (1965).
[2] J. M. Luttinger, New mechanism for superconductivity, Phys. Rev. **150**, 202 (1966).
[3] S. Miyahara, S. Kusuta, and N. Furukawa, BCS theory on a flat band lattice, Physica C: Superconductivity **460-462**, 1145 (2007).
[4] S. Zhang, H.-h. Hung, and C. Wu, Proposed realization of itinerant ferromagnetism in optical lattices, Phys. Rev. A **82**, 053618 (2010).
[5] C. Wu, D. Bergman, L. Balents, and S. Das Sarma, Flat Bands and Wigner Crystallization in the Honeycomb Optical Lattice, Phys. Rev. Lett. **99**, 070401 (2007).
[6] T. Neupert, L. Santos, C. Chamon, and C. Mudry, Fractional Quantum Hall States at Zero Magnetic Field, Phys. Rev. Lett. **106**, 236804 (2011).
[7] D. N. Sheng, Z.-C. Gu, K. Sun, and L. Sheng, Fractional quantum hall effect in the absence of landau levels, Nat. Commun. **2**, 389 (2011).
[8] K. Sun, Z. Gu, H. Katsura, and S. Das Sarma, Nearly Flatbands with Nontrivial Topology, Phys. Rev. Lett. **106**, 236803 (2011).
[9] N. Regnault and B. A. Bernevig, Fractional Chern Insulator, Phys. Rev. X **1**, 021014 (2011).
[10] Z. Liu, Z.-F. Wang, J.-W. Mei, Y.-S. Wu, and F. Liu, Flat Chern Band in a Two-Dimensional Organometallic Framework, Phys. Rev. Lett. **110**, 106804 (2013).

[11] D.-B. Zhang, X.-J. Zhao, G. Seifert, K. Tse, and J. Zhu, Twist-driven separation of p-type and n-type dopants in single-crystalline nanowires, Natl. Sci. Rev. **6**, 532 (2019).
[12] X.-J. Zhao, G. Seifert, J. Zhu, and D.-B. Zhang, Twist-induced preferential distribution of dopants in single-crystalline si nanowires, Phys. Rev. B **100**, 174202 (2019).
[13] Y. Cao, V. Fatemi, A. Demir, S. Fang, S. L. Tomarken, J. Y. Luo, J. D. Sanchez-Yamagishi, K. Watanabe, T. Taniguchi, E. Kaxiras, R. C. Ashoori, and P. Jarillo-Herrero, Correlated insulator behavior at half-filling in magic-angle graphene superlattices, Nature (London) **556**, 80 (2018).
[14] Y. Cao, V. Fatemi, S. Fang, K. Watanabe, T. Taniguchi, E. Kaxiras, and P. Jarillo-Herrero, Unconventional superconductivity in magic-angle graphene superlattices, Nature (London) **556**, 43 (2018).
[15] M. Yankowitz, S. Chen, H. Polshyn, Y. Zhang, K. Watanabe, T. Taniguchi, D. Graf, A. F. Young, and C. R. Dean, Tuning superconductivity in twisted bilayer graphene, Science **363**, 1059 (2019).
[16] C. R. Dean, L. Wang, P. Maher, C. Forsythe, F. Ghahari, Y. Gao, J. Katoch, M. Ishigami, P. Moon, M. Koshino, T. Taniguchi, K. Watanabe, K. L. Shepard, J. Hone, and P. Kim, Hofstadter's butterfly and the fractal quantum hall effect in moiré superlattices, Nature (London) **497**, 598 (2013).
[17] B. Hunt, J. D. Sanchez-Yamagishi, A. F. Young, M. Yankowitz, B. J. LeRoy, K. Watanabe, T. Taniguchi, P. Moon, M. Koshino, P. Jarillo-Herrero, and R. C. Ashoori, Massive dirac fermions and hofstadter butterfly in a van der Waals heterostructure, Science **340**, 1427 (2013).
[18] E. M. Spanton, A. A. Zibrov, H. Zhou, T. Taniguchi, K. Watanabe, M. P. Zaletel, and A. F. Young, Observation of fractional chern insulators in a van der waals heterostructure, Science **360**, 62 (2018).
[19] J. C. W. Song, A. V. Shytov, and L. S. Levitov, Electron Interactions and Gap Opening in Graphene Superlattices, Phys. Rev. Lett. **111**, 266801 (2013).
[20] K. L. Seyler, P. Rivera, H. Yu, N. P. Wilson, E. L. Ray, D. G. Mandrus, J. Yan, W. Yao, and X. Xu, Signatures of moiré-trapped valley excitons in $MoSe_2/WSe_2$ heterobilayers, Nature (London) **567**, 66 (2019).
[21] K. Tran, G. Moody, F. Wu, X. Lu, J. Choi, K. Kim, A. Rai, D. A. Sanchez, J. Quan, A. Singh, J. Embley, A. Zepeda, M. Campbell, T. Autry, T. Taniguchi, K. Watanabe, N. Lu, S. K. Banerjee, K. L. Silverman, S. Kim, E. Tutuc, L. Yang, A. H. MacDonald, and X. Li, Evidence for moiré excitons in van der Waals heterostructures, Nature (London) **567**, 71 (2019).
[22] C. Jin, E. C. Regan, A. Yan, M. Iqbal Bakti Utama, D. Wang, S. Zhao, Y. Qin, S. Yang, Z. Zheng, S. Shi, K. Watanabe, T. Taniguchi, S. Tongay, A. Zettl, and F. Wang, Observation of moiré excitons in WSe_2/WS_2 heterostructure superlattices, Nature (London) **567**, 76 (2019).
[23] E. M. Alexeev, D. A. Ruiz-Tijerina, M. Danovich, M. J. Hamer, D. J. Terry, P. K. Nayak, S. Ahn, S. Pak, J. Lee, J. I. Sohn, M. R. Molas, M. Koperski, K. Watanabe, T. Taniguchi, K. S. Novoselov, R. V. Gorbachev, H. S. Shin, V. I. Fal'ko, and A. I. Tartakovskii, Resonantly hybridized excitons in moiré superlattices in van der Waals heterostructures, Nature (London) **567**, 81 (2019).
[24] R. Bistritzer and A. H. MacDonald, Moiré bands in twisted double-layer graphene, Proc. Natl. Acad. Sci. USA **108**, 12233 (2011).
[25] J. M. B. Lopes dos Santos, N. M. R. Peres, and A. H. Castro Neto, Continuum model of the twisted graphene bilayer, Phys. Rev. B **86**, 155449 (2012).
[26] G. Trambly de Laissardière, D. Mayou, and L. Magaud, Numerical studies of confined states in rotated bilayers of graphene, Phys. Rev. B **86**, 125413 (2012).
[27] S. Fang and E. Kaxiras, Electronic structure theory of weakly interacting bilayers, Phys. Rev. B **93**, 235153 (2016).
[28] S. Carr, S. Fang, P. Jarillo-Herrero, and E. Kaxiras, Pressure dependence of the magic twist angle in graphene superlattices, Phys. Rev. B **98**, 085144 (2018).
[29] B. L. Chittari, N. Leconte, S. Javvaji, and J. Jung, Pressure induced compression of flatbands in twisted bilayer graphene, Electron. Struct. **1**, 015001 (2018).
[30] A. Ramires and J. L. Lado, Electrically Tunable Gauge Fields in Tiny-Angle Twisted Bilayer Graphene, Phys. Rev. Lett. **121**, 146801 (2018).
[31] F. Wu, T. Lovorn, E. Tutuc, and A. H. MacDonald, Hubbard Model Physics in Transition Metal Dichalcogenide Moiré Bands, Phys. Rev. Lett. **121**, 026402 (2018).
[32] M. H. Naik and M. Jain, Ultraflatbands and Shear Solitons in Moiré Patterns of Twisted Bilayer Transition Metal Dichalcogenides, Phys. Rev. Lett. **121**, 266401 (2018).
[33] X.-J. Zhao, Y. Yang, D.-B. Zhang, and S.-H. Wei, Formation of Bloch Flat Bands in Polar Twisted Bilayers Without Magic Angles, Phys. Rev. Lett. **124**, 086401 (2020).
[34] D. Porezag, T. Frauenheim, T. Köhler, G. Seifert, and R. Kaschner, Construction of tight-binding-like potentials on the basis of density-functional theory: Application to carbon, Phys. Rev. B **51**, 12947 (1995).
[35] R. Rurali and E. Hernandez, Trocadero: A multiple-algorithm multiple-model atomistic simulation program, Comput. Mater. Sci. **28**, 85 (2003).
[36] P. Hohenberg and W. Kohn, Inhomogeneous electron gas, Phys. Rev. **136**, B864 (1964).
[37] G. Kresse and J. Hafner, *Ab initio* molecular-dynamics simulation of the liquid-metal–amorphous-semiconductor transition in germanium, Phys. Rev. B **49**, 14251 (1994).
[38] P. E. Blöchl, Projector augmented-wave method, Phys. Rev. B **50**, 17953 (1994).
[39] J. P. Perdew, K. Burke, and M. Ernzerhof, Generalized Gradient Approximation Made Simple, Phys. Rev. Lett. **77**, 3865 (1996).
[40] C. Tusche, H. L. Meyerheim, and J. Kirschner, Observation of Depolarized ZnO(0001) Monolayers: Formation of Unreconstructed Planar Sheets, Phys. Rev. Lett. **99**, 026102 (2007).
[41] H.-Q. Song, Z. Liu, and D.-B. Zhang, Interlayer vibration of twisted bilayer graphene: A first-principles study, Phys. Lett. A **383**, 2628 (2019).
[42] P. Moon and M. Koshino, Energy spectrum and quantum hall effect in twisted bilayer graphene, Phys. Rev. B **85**, 195458 (2012).
[43] V. V. Enaldiev, V. Zólyomi, C. Yelgel, S. J. Magorrian, and V. I. Fal'ko, Stacking Domains and Dislocation Networks in Marginally Twisted Bilayers of Transition Metal Dichalcogenides, Phys. Rev. Lett. **124**, 206101 (2020).

[44] A. Weston, Y. Zou, V. Enaldiev, A. Summerfield, N. Clark, V. Zólyomi, A. Graham, C. Yelgel, S. Magorrian, M. Zhou, J. Zultak, D. Hopkinson, A. Barinov, T. H. Bointon, A. Kretinin, N. R. Wilson, P. H. Beton, V. I. Fal'ko, S. J. Haigh, and R. Gorbachev, Atomic reconstruction in twisted bilayers of transition metal dichalcogenides, Nat. Nanotechnol. **15**, 592 (2020).

[45] M. R. Rosenberger, H.-J. Chuang, M. Phillips, V. P. Oleshko, K. M. McCreary, S. V. Sivaram, C. S. Hellberg, and B. T. Jonker, Twist angle-dependent atomic reconstruction and moiré patterns in transition metal dichalcogenide heterostructures, ACS Nano **14**, 4550 (2020).

[46] H. Sahin, S. Cahangirov, M. Topsakal, E. Bekaroglu, E. Akturk, R. T. Senger, and S. Ciraci, Monolayer honeycomb structures of group-IV elements and III-V binary compounds: First-principles calculations, Phys. Rev. B **80**, 155453 (2009).

[47] R. Saito, G. Dresselhaus, and M. S. Dresselhaus, *Physical Properties of Carbon Nanotubes* (Imperial College Press, London, 1998), pp. 17–33.